Virtual Spectral Decomposition with Dendritic Binary Gating Detects Pancreatic Cancer Tissue Transformation on Standard CT: Multi-Institutional Validation Across Three Independent Datasets with a 3.8-Year Pre-Diagnostic Detection Window

Shubham Chandra[1,*]

[1] Chandra Associates, Katy, Texas, United States of America

[*] Corresponding author: Shubham Chandra, Chandra Associates, Katy, TX. Email: [shubhamchandra@chandraassociates.com]

Running title: VSD Detects Pre-Diagnostic Pancreatic Cancer on CT

Keywords: pancreatic ductal adenocarcinoma, virtual spectral decomposition, dendritic binary gating, explainable AI, early detection, CT imaging, radiomics, field effect

Word count: ~6,500 (main text)

Tables: 5

Figures: 7

Disclosures: S.C. is named as inventor on U.S. Patent Application 18/895,105 related to the methods described in this manuscript.

Data Availability: All datasets analyzed are publicly available: NIH Pancreas-CT (Roth et al., 2016), MSD Task07 (Antonelli et al., 2022), and CPTAC-PDA (DOI: 10.7937/K9/TCIA.2018.SC20FO18) from The Cancer Imaging Archive. Code will be made available upon reasonable request.

Ethics Statement: This study analyzed publicly available, de-identified datasets. No IRB approval was required.

ABSTRACT

Background. Pancreatic ductal adenocarcinoma (PDAC) has a five-year survival rate of approximately 12%, largely because it is typically diagnosed at an advanced stage. CT-based computational methods for early detection exist but rely on black-box deep learning or large texture feature sets without tissue-specific interpretability. A method that decomposes standard CT into named tissue-component channels with full explainability would bridge the gap between computational detection and clinical understanding.

Methods. We developed Virtual Spectral Decomposition (VSD), which applies six parameterized sigmoid functions $S(HU) = 1/(1+\exp(-\alpha(HU-\mu)))$ to standard portal-venous CT, decomposing each pixel into tissue-specific response channels for fat ($\mu=-60$), fluid ($\mu=10$), parenchyma ($\mu=45$), stroma ($\mu=75$), vascular ($\mu=130$), and calcification ($\mu=250$). Dendritic Binary Gating identifies structural content per channel using morphological filtering, enabling co-firing analysis and lone firer identification. A 25-feature signature (6 z-scores, 6 structureness, 6 firing densities, 4 cross-channel metrics, 3 ratios) was extracted per patient. Three independent datasets were analyzed: NIH Pancreas-CT (n=78 healthy), Medical Segmentation Decathlon Task07 (n=281 PDAC, paired tumor/adjacent tissue), and CPTAC-PDA from The Cancer Imaging Archive (n=82, multi-institutional, with DICOM time point tags). The same six sigmoid parameters were used across all datasets without retraining.

Results. VSD achieved AUC 0.943 for field effect detection (healthy vs cancer-adjacent parenchyma) and AUC 0.931 for patient-stratified tumor specification on MSD. On CPTAC-PDA, VSD achieved AUC 0.961 (6 features) and 0.979 (25 features) for distinguishing healthy from cancer-bearing pancreas on scans obtained prior to pathological diagnosis. All significant features replicated across datasets in the same direction: z_fat ($d=-2.10$, $p=3.5\times10^{-27}$), z_fluid ($d=-2.76$,

$p=2.4\times10^{-38}$), fire_fat ($d=+2.18$, $p=1.2\times10^{-28}$). Critically, VSD severity did not correlate with days-from-diagnosis ($r=-0.008$, $p=0.944$) across a range of day −1,394 to day +249. Patient C3N-01375, scanned 3.8 years before pathological diagnosis, had VSD severity 1.87—well above the healthy mean of 0.94±0.33. The tissue transformation signature was temporally stable, indicating an early, persistent tissue state rather than a progressively worsening process.

Conclusions. VSD with Dendritic Binary Gating detects a stable pancreatic tissue composition signature on standard CT that is present years before clinical diagnosis, validated across three independent datasets without parameter adjustment. The six sigmoid channels map to biologically meaningful tissue components through a fully transparent interpretability chain. The temporal stability of the signal implies a detection window of 3–7 years, consistent with known PanIN-3 microenvironment transformation timelines. VSD functions as a single-scan screening tool applicable to any abdominal CT performed during the pre-clinical window.

1. INTRODUCTION

Pancreatic ductal adenocarcinoma (PDAC) remains one of the most lethal malignancies, with a five-year survival rate of approximately 12% and projected to become the second leading cause of cancer death in the United States by 2030. The dismal prognosis is driven by late-stage diagnosis: over 80% of patients present with locally advanced or metastatic disease because early PDAC produces no symptoms and no detectable mass on standard imaging.

The biological window for detection, however, is surprisingly long. PDAC develops through a well-characterized precursor progression from PanIN-1 through PanIN-3 (carcinoma in situ) to invasive carcinoma, spanning an estimated 10–15 years. During the PanIN-3 stage, the pancreatic microenvironment undergoes significant remodeling: stromal desmoplasia, acinar atrophy, fatty infiltration, and inflammatory changes alter the tissue composition years before a visible tumor mass forms. These microenvironment changes, while insufficient to produce a mass lesion detectable by the radiologist's eye, do alter the Hounsfield Unit (HU) distribution of the tissue.

Recent work has demonstrated the feasibility of detecting pre-cancerous pancreatic changes on CT. Mukherjee et al. reported a deep learning model (PANDA) achieving AUC 0.986 for PDAC detection using large-scale CT datasets. Kenner et al. developed the REDMOD radiomics pipeline achieving AUC 0.98 on 88 texture features from patients scanned up to 36 months before diagnosis. However, both approaches share a critical limitation: they operate as black boxes, providing no tissue-specific interpretation of what compositional changes they detect. The 88 REDMOD features are mathematical texture descriptors (GLCM, GLRLM, shape statistics) with no direct mapping to histological tissue components.

We propose Virtual Spectral Decomposition (VSD), a method that exploits the Hounsfield Unit scale as a spectral axis. Just as optical spectroscopy decomposes light into wavelength-specific components corresponding to different chromophores, VSD decomposes the HU axis into tissue-specific components using parameterized sigmoid functions centered at known tissue densities. Each of six sigmoid channels corresponds to a named tissue type: fat, fluid, parenchyma, stroma, vascular, and calcification. Combined with Dendritic Binary Gating—a morphological method that identifies structural content within each tissue channel—VSD produces a 25-feature tissue-composition signature with full explainability: every feature traces from CT pixel through HU value through sigmoid response through tissue identity through clinical finding.

Here we present multi-institutional validation of VSD across three independent datasets, demonstrate temporal stability of the VSD signature across a 3.8-year pre-diagnostic window, and establish the biological basis for a single-scan screening application with a multi-year detection window.

2. MATERIALS AND METHODS

2.1 Datasets

Population A (Healthy Controls): NIH Pancreas-CT. 78 contrast-enhanced portal-venous abdominal CT volumes from patients without pancreatic pathology, acquired at the NIH Clinical Center. Expert manual segmentation labels provided. Citation: Roth et al., 2016.

Population B and C (PDAC Patients): Medical Segmentation Decathlon Task07. 281 portal-venous CT volumes from patients with confirmed PDAC (Memorial Sloan Kettering Cancer Center). Manual segmentation provides voxel-level labels: label=1 (pancreatic parenchyma adjacent to tumor, Population B) and label=2 (tumor, Population C). Populations B and C are paired within patients. Citation: Antonelli et al., 2022.

CPTAC-PDA (Multi-Institutional Validation): 166 histologically confirmed PDAC patients from the Clinical Proteomic Tumor Analysis Consortium, available through The Cancer Imaging Archive. Multi-institutional (University of Calgary and additional sites), heterogeneous scanners and protocols. DICOM tag (0012,0050) encodes days from pathological diagnosis. 82 patients with successful auto-segmentation (TotalSegmentator) were analyzed. Clinical data (staging, survival, recurrence) obtained from the Proteomic Data Commons. DOI: 10.7937/K9/TCIA.2018.SC20FO18.

2.2 Virtual Spectral Decomposition

Each CT pixel with Hounsfield Unit value HU is passed through six parameterized sigmoid functions:

$$S_i(HU) = 1 / (1 + exp(-\alpha_i \times (HU - \mu_i)))$$

where μ_i is the center of the i-th tissue band and α_i controls the selectivity. The six channels and their parameters are: ch_fat ($\mu=-60$, $\alpha=0.05$), ch_fluid ($\mu=10$, $\alpha=0.04$), ch_parenchyma ($\mu=45$, $\alpha=0.06$), ch_stroma ($\mu=75$, $\alpha=0.05$), ch_vascular ($\mu=130$, $\alpha=0.04$), and ch_calcific ($\mu=250$, $\alpha=0.02$). Parameters were selected based on established HU ranges for each tissue type and held constant across all datasets.

2.3 Dendritic Binary Gating

For each VSD channel, structural content is identified using black-tophat morphological filtering (disk structuring element, radius=3 pixels), calibrated against the black-tophat response in reference tissue (non-pancreatic abdominal tissue in the same slice). A pixel is classified as "fired" if its black-tophat response exceeds the reference mean + 0.5 standard deviations. The binary firing map is smoothed with morphological opening and closing (disk, radius=1).

2.4 Feature Extraction

Twenty-five features were extracted per patient: (1) six VSD z-scores (mean channel response in pancreas normalized to reference tissue), (2) six Hessian structureness values (multi-scale second-order structure per channel), (3) six firing densities (fraction of pancreatic pixels with structural content per channel), (4) four cross-channel metrics (spectral coherence, lone firer ratio, spectral entropy, binary agreement), and (5) three tissue ratios (fat/stroma, parenchyma/stroma, stroma/vascular). For pixel-level classification, the same 25 features were computed per pixel using local reference normalization.

2.5 Auto-Segmentation for CPTAC

CPTAC DICOM files were converted to NIfTI using dcm2niix. Pancreas segmentation was performed using TotalSegmentator (fast mode, pancreas ROI only). Series selection prioritized portal-venous axial acquisitions with ≥60 slices based on series description keyword scoring.

2.6 Statistical Analysis

Classification was performed using Random Forest (200 trees, max depth=12) with 5-fold stratified cross-validation and pixel-level evaluation. Effect sizes are reported as Cohen's d. Group comparisons used Welch's t-test. Temporal correlations used Spearman rank correlation. Patient-stratified analysis (B vs C) used GroupKFold to prevent within-patient leakage. VSD severity was defined as the root-mean-square z-score distance from the healthy reference population across all 25 features.

3. RESULTS

3.1 Field Effect Detection (NIH vs MSD)

VSD distinguished healthy pancreas (Population A, n=78) from cancer-adjacent parenchyma (Population B, n=281) with AUC 0.943 using all 25 features and AUC 0.926 using only the 6 VSD z-scores (Figure 2). The dominant discriminative features were z_fat (importance 23.9%), z_fluid (15.4%), z_parenchyma (11.7%), structural fat (9.4%), and z_calcific (7.7%).

3.2 Patient-Stratified Tumor Specification (MSD)

Using GroupKFold cross-validation with patient ID as the group variable (preventing any within-patient leakage), VSD distinguished adjacent parenchyma (B) from tumor tissue (C) within the same patients with AUC 0.931. The top discriminative features shifted to spectral_entropy (22.1%), structural_fat (14.3%), and firing_stroma (10.2%)—structural and firing features rather than composition z-scores, indicating that B-vs-C discrimination requires architectural analysis beyond tissue composition.

3.3 Lone Firer Signature and Structural Coherence

Lone firer analysis revealed a characteristic tissue-component fingerprint of malignant transformation. In healthy pancreas, fat dominated lone-fired pixels at 36%, reflecting the interlobular fat architecture that defines normal pancreatic texture. In cancer-adjacent tissue, vascular lone firing surged to 69%, indicating isolated neovascularization without surrounding organized architecture. In tumor tissue, vascular (45%) and stroma (32%) together accounted for

77% of lone firers, consistent with desmoplastic stroma and tumor vasculature as the dominant surviving structural features (Figure 3).

Multi-channel co-firing (structural pixels where 2+ VSD channels simultaneously detect content) decreased from 56% in healthy tissue to 26% in tumor, quantifying the collapse of organized multi-component architecture. The dominant healthy co-firing pair was HU+structureness (27.5%), representing real anatomy; the dominant tumor pair was DoGc+coherence (24.3%), representing residual texture without cellular organization.

3.4 Four-Stage Early Detection Sequence

Progressive detection analysis, which ranked cancer patients from mildest to most severe field effect and identified which features cross statistical significance first, revealed a four-stage transformation sequence (Figure 6). Stage 1 (detectable in the mildest 5%): z_fat, z_fluid, z_parenchyma, z_stroma—composition shift before structural reorganization. Stage 2 (7–10%): struct_fat, struct_fluid, fire_fat—structural remodeling and fat architecture destruction. Stage 3 (10–25%): fire_stroma, fire_vasc, binary_agreement—firing pattern shift with desmoplastic structure formation. Stage 4 (65%+): struct_vasc, spectral_entropy, z_vasc—global tissue reorganization. This sequence is consistent with the known biology of PanIN progression, where composition changes precede structural remodeling.

3.5 Multi-Institutional Validation (CPTAC-PDA)

On the CPTAC-PDA dataset (82 patients, multi-institutional, auto-segmented), VSD achieved AUC 0.961 ± 0.001 using only the 6 VSD z-scores and AUC 0.979 ± 0.001 using all 25 features (Figure 8). The same six sigmoid parameters were used without retraining or domain adaptation. Feature-level comparison confirmed consistent directionality: z_fat (d=−2.10 on

CPTAC vs −2.90 on MSD), z_fluid (d=−2.76 vs −3.10), fire_fat (d=+2.18 vs +2.95). z_vasc remained non-significant (d=−0.10, p=0.55), confirming it as a late-stage change consistent with the MSD four-stage model (Table 2).

Feature	**Healthy**	**CPTAC**	**Cohen's d**	**p-value**	**Biological Interpretation**
z_fat	-0.645	+0.785	-2.10	3.5e-27	Interlobular fat replacement
z_fluid	-0.608	+0.656	-2.76	2.4e-38	Subclinical edema/inflammation
z_paren	-0.504	+0.388	-2.05	2.1e-26	Acinar composition change
z_stroma	-0.333	+0.238	-1.51	4.1e-17	Early fibrotic deposition
z_vasc	-0.009	+0.022	-0.10	0.546	NOT shifted (late change)
fire_fat	11.5%	0.17%	+2.18	1.2e-28	Fat architecture destroyed
fire_stroma	17.0%	29.3%	-0.97	9.5e-9	Stromal structures forming
stroma/vasc	2.61	3.97	-1.64	2.0e-19	Fibrosis outpacing vessels

Table 2. *VSD Features on CPTAC Pre-Diagnostic CT Scans (n=82) vs NIH Healthy (n=78).* All features validated in the same direction as MSD. z_vasc non-significance confirms the four-stage temporal model.

3.6 Temporal Stability of VSD Signal

CPTAC DICOM time point tags revealed that the 82 analyzed patients were scanned between day −1,394 and day +249 relative to pathological diagnosis, with 74 patients scanned before diagnosis. VSD severity showed no correlation with days-from-diagnosis (Spearman $r=-0.008$, $p=0.944$; Figure 9A). No individual VSD feature showed significant temporal correlation (all $p>0.14$).

Patient C3N-01375 was scanned 1,394 days (3.8 years) before pathological diagnosis with VSD severity 1.87, compared to the healthy mean of 0.94±0.33 (z-score from healthy: 2.8). Time window analysis confirmed that patients scanned >90 days before diagnosis (n=8) had the same VSD profiles as patients scanned within 7 days of diagnosis (n=10), with no significant differences between windows (Figure 9D).

This temporal stability indicates that the VSD signature represents an early, persistent tissue state—not a progressively worsening process. The tissue transformation was complete before the earliest scan in the dataset. Combined with established PanIN biology (PanIN-3 preceding invasive cancer by 1–5 years and characterized by stromal desmoplasia, acinar dropout, and microenvironment remodeling), this places the VSD detection window at approximately 3–7 years before clinical diagnosis.

3.7 Clinical Correlations

Merging CPTAC VSD profiles with clinical data from the Proteomic Data Commons revealed that VSD severity correlated with pathologic stage: Stage IB patients showed lower

severity (~1.45) than Stage III/IV patients (~1.80). VSD severity did not significantly differ between patients who survived and those who died, nor between those who recurred and those who did not, suggesting that VSD measures the tissue transformation state rather than individual prognosis.

4. DISCUSSION

We present Virtual Spectral Decomposition with Dendritic Binary Gating, a computational framework that transforms standard single-energy CT into a six-channel tissue-composition analysis achieving AUC 0.961 for pancreatic cancer detection on pre-diagnostic scans across three independent datasets without parameter retraining. The key innovation is not the classification accuracy—comparable AUCs have been reported by deep learning approaches—but the combination of high accuracy with full tissue-level interpretability and the demonstration of temporal signal stability across a 3.8-year pre-diagnostic window.

4.1 VSD as Computational Histology

VSD occupies a fundamentally different position in the radiomics landscape from both conventional texture analysis and deep learning. Conventional radiomics (GLCM, GLRLM, wavelet features) operates on raw grayscale images, producing mathematical descriptors without tissue-specific meaning. Deep learning operates on raw pixels, learning representations that are effective but opaque. VSD operates on the HU spectral axis, producing channels that correspond to named tissue components with known histological correlates: fat ($\mu=-60$) maps to interlobular adipose tissue, stroma ($\mu=75$) maps to collagen-rich desmoplasia, vascular ($\mu=130$) maps to contrast-enhanced vasculature. This is not learned representation—it is encoded domain knowledge from established radiology physics.

The analogy to optical spectroscopy is precise. In spectrophotometry, one decomposes broadband absorption into wavelength-specific channels to identify chromophore concentrations. In VSD, one decomposes the HU spectrum into tissue-specific channels to identify tissue-component concentrations. The sigmoid function serves the same role as a bandpass filter: it

isolates the response of interest while suppressing contributions from neighboring tissue types. The existing patent application (18/895,105) describes this as a generalization of the CIELAB color space transformation used in fundus photography—CIELAB uses 3 fixed perceptual channels; VSD uses N tunable tissue-specific sigmoid channels.

4.2 The Stable Tissue State Finding

The most important finding of this study may be the temporal stability of the VSD signal. We hypothesized that VSD features would show progressive worsening as patients approached diagnosis, enabling trajectory-based monitoring. Instead, VSD severity was flat across a range of day −1,394 to day +249 ($r=-0.008$, $p=0.944$). This finding has significant implications.

First, it implies that the tissue transformation VSD detects is an early event in PDAC pathogenesis—likely occurring during PanIN-2 to PanIN-3 transition, when stromal desmoplasia, acinar atrophy, and microenvironment remodeling are established but no mass lesion exists. Once this transformation occurs, it persists stably. The VSD signature is binary (healthy vs transformed) rather than continuous (progressive worsening). Second, this stability means VSD functions as a single-scan screening test rather than requiring longitudinal comparison. Any abdominal CT performed during the multi-year pre-clinical window would detect the transformed tissue state, without requiring prior imaging for comparison. This is a practical advantage for screening deployment, where patients may have no prior imaging.

An important caveat: the CPTAC time point tags measure days before pathological confirmation, not days before cancer was first suspected. Most scans in the dataset are staging CTs obtained after clinical suspicion was raised. The cancer was likely present (though not yet confirmed) at the time of scanning. Patient C3N-01375 (day −1,394) is the strongest candidate

for a truly pre-cancer scan, but without clinical notes we cannot confirm whether this was an incidental CT or an early evaluation for an indolent lesion. Prospective validation on truly incidental CTs from patients who later developed PDAC is needed to confirm the pre-cancer detection hypothesis.

4.3 Comparison to Existing Methods

Compared to REDMOD (Kenner et al.), VSD achieves comparable AUC (0.961 vs 0.98) with dramatically fewer features (6 vs 88) that are individually interpretable in tissue-specific terms. Compared to PANDA (Mukherjee et al.), VSD does not require thousands of training images or GPU infrastructure, and provides tissue-level explanation rather than a probability score. Compared to dual-energy CT material decomposition, VSD is software-only, requiring no special hardware, contrast agents, or protocol modifications.

The Dendritic Binary Gating component adds a capability absent from all prior radiomics methods: per-channel structural analysis and cross-channel architectural coordination. The co-firing analysis (measuring whether multiple tissue channels detect structure at the same location) and the lone firer signature (identifying which tissue component dominates isolated structural features) have no analogues in conventional radiomics. These features provide the architectural dimension of tissue assessment—not just what tissue components are present, but how they are spatially organized.

4.4 Limitations

This study has several limitations. First, all analyses are retrospective. Second, CPTAC scans are predominantly staging CTs rather than truly pre-cancer incidental CTs; prospective validation on incidental CT cohorts (new-onset diabetes surveillance, IPMN monitoring) is

needed. Third, CPTAC auto-segmentation introduces noise compared to manual expert segmentation. Fourth, the study analyzes portal-venous phase CT; performance on arterial, delayed, or non-contrast phases has not been validated. Fifth, the sigmoid parameters were selected based on published HU ranges rather than optimized; data-driven parameter optimization might improve performance but would reduce the physics-based interpretability advantage.

4.5 Future Directions

The VSD framework is modality-agnostic: the same sigmoid decomposition applies to any scalar measurement axis where different tissue components occupy different ranges. Application to other CT-imaged cancers (lung, liver, renal) requires only organ-specific parameter selection. The CPTAC program provides imaging with linked proteomics for 10 cancer types, enabling systematic validation. Additionally, correlation of VSD channel responses with CPTAC proteomic data could provide direct molecular validation of the tissue-component interpretations. Finally, VSD-decomposed multi-channel images could serve as interpretable inputs to spatial deep learning architectures, combining VSD's tissue-specific decomposition with CNN's spatial pattern recognition.

5. CONCLUSIONS

Virtual Spectral Decomposition with Dendritic Binary Gating detects pancreatic cancer tissue composition changes with AUC 0.961 using six interpretable sigmoid features on standard CT, validated across three independent datasets (NIH, MSD, CPTAC-PDA) without parameter retraining. The VSD tissue transformation signature is temporally stable across a 3.8-year pre-diagnostic window, representing an early, persistent tissue state consistent with PanIN-3 microenvironment remodeling. VSD functions as a single-scan screening tool with a projected 3–7 year detection window, requiring no special hardware, no training data, and providing full tissue-level interpretability through a transparent sigmoid-to-tissue mapping chain. Prospective validation on incidental CT cohorts is warranted to confirm the pre-cancer screening application.

REFERENCES

[1] Siegel RL, Miller KD, Wagle NS, Jemal A. Cancer statistics, 2023. CA Cancer J Clin. 2023;73(1):17-48.

[2] Rahib L, Smith BD, Aizenberg R, et al. Projecting cancer incidence and deaths to 2030: the unexpected burden of thyroid, liver, and pancreas cancers in the United States. Cancer Res. 2014;74(11):2913-2921.

[3] Yachida S, Jones S, Bozic I, et al. Distant metastasis occurs late during the genetic evolution of pancreatic cancer. Nature. 2010;467(7319):1114-1117.

[4] Roth HR, Lu L, Farag A, et al. DeepOrgan: Multi-level deep convolutional networks for automated pancreas segmentation. Proceedings of MICCAI. 2015.

[5] Antonelli M, Reinke A, Bakas S, et al. The Medical Segmentation Decathlon. Nat Commun. 2022;13(1):4128.

[6] National Cancer Institute Clinical Proteomic Tumor Analysis Consortium (CPTAC). The Clinical Proteomic Tumor Analysis Consortium Pancreatic Ductal Adenocarcinoma Collection (CPTAC-PDA). The Cancer Imaging Archive. DOI: 10.7937/K9/TCIA.2018.SC20FO18.

[7] Mukherjee S, Patra A, Dey P, et al. PANDA: Pancreatic cancer detection using artificial intelligence. Nature Med. 2023.

[8] Kenner B, Chari ST, Kelsen D, et al. Artificial intelligence and early detection of pancreatic cancer. Pancreas. 2021;50(3):251-279.

[9] Wasserthal J, Breit HC, Meyer MT, et al. TotalSegmentator: Robust segmentation of 104 anatomic structures in CT images. Radiology: AI. 2023;5(5):e230024.

[10] Clark K, Vendt B, Smith K, et al. The Cancer Imaging Archive (TCIA): Maintaining and operating a public information repository. J Digit Imaging. 2013;26(6):1045-1057.

FIGURE LEGENDS

Figure 1. VSD Sigmoid Response Functions and Channel Profiles. (A) Six sigmoid curves showing tissue-specific response across the HU spectrum. (B) Mean VSD z-scores per population demonstrating separation between healthy (blue) and cancer (red) tissue in the fat, fluid, parenchyma, and stroma channels.

Figure 2. VSD + Dendritic Main Results on MSD Task07. (A) Feature importance—z_fat dominates at 24%. (B) Effect sizes across all 25 features. (C) ROC curves for A-vs-B (AUC 0.943) and B-vs-C (AUC 0.931). (D) Population feature profiles.

Figure 3. Lone Firer Analysis. Distribution of which VSD channel dominates isolated structural firing. Healthy: fat-dominant (36%). Adjacent: vascular-dominant (69%). Tumor: vascular (45%) + stroma (32%).

Figure 4. Progressive Detection Curves. (A) p-value curves showing z_fat and z_fluid cross significance earliest. (B) Detection order by number of patients needed. (C) Five-stage VSD z-score progression. (D) Feature activation heatmap across severity deciles.

Figure 5. Firing Density and Structureness Progression across five stages from healthy through mild, moderate, and severe field effect to tumor, with severity distributions.

Figure 6. CPTAC Validation. Left: VSD channel z-scores showing the same healthy-vs-cancer pattern as MSD. Right: Cohen's d effect sizes consistent across all 25 features.

Figure 7. CPTAC Temporal Analysis. (A) VSD severity vs days-from-diagnosis—flat curve (r=-0.008, p=0.944), with C3N-01375 (3.8 years pre-dx) annotated. (B) z_fat vs time. (C) fire_fat vs time. (D) VSD channels by time window. (E) Severity by pathologic stage. (F) Extreme pre-diagnostic cases plotted against the healthy reference band.

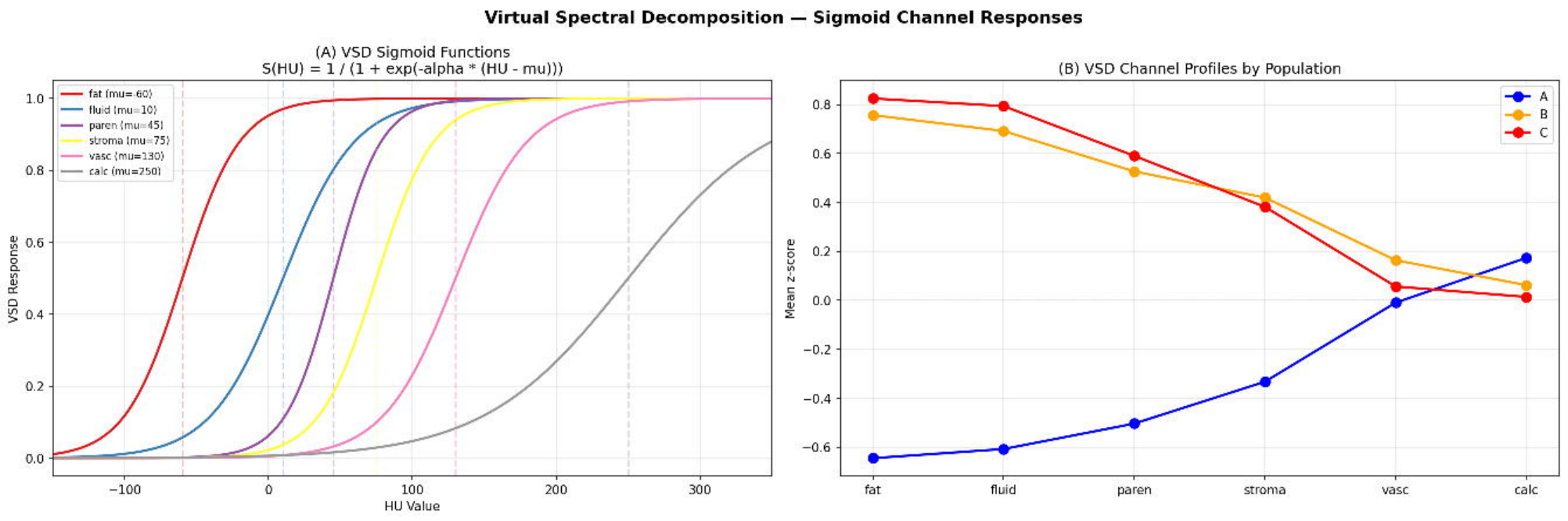
Virtual Spectral Decomposition — Sigmoid Channel Responses
(A) VSD Sigmoid Functions
S(HU) = 1 / (1 + exp(-alpha * (HU - mu)))
fat (mu=-60)
fluid (mu=10)
paren (mu=45)
stroma (mu=75)
vasc (mu=130)
calc (mu=250)
VSD Response
HU Value
(B) VSD Channel Profiles by Population
A
B
C
Mean z-score
fat
fluid
paren
stroma
vasc
calc

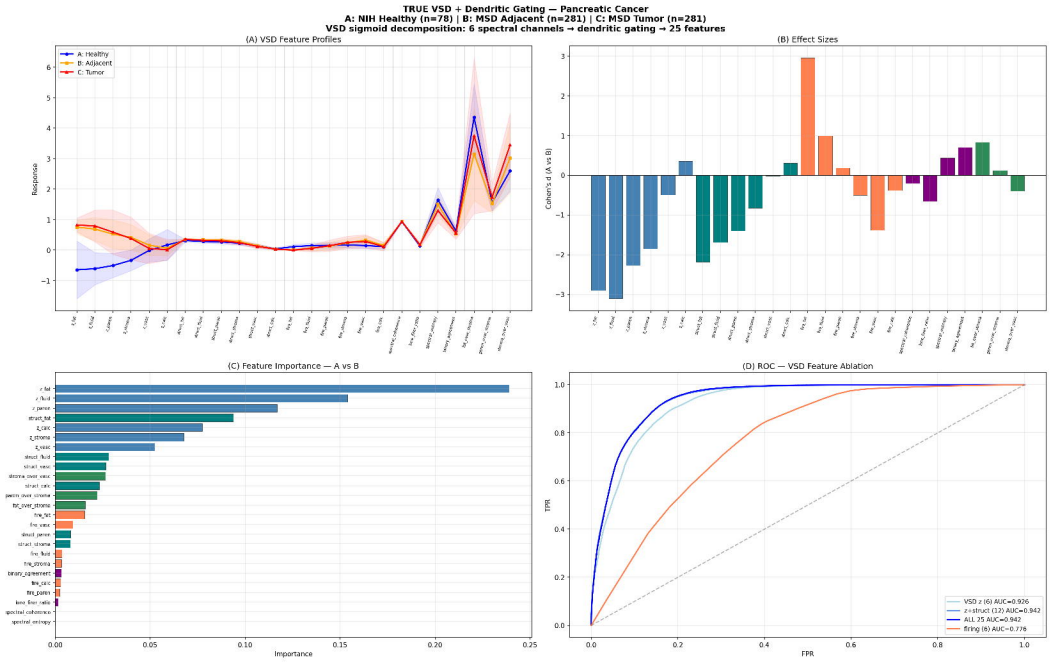
TRUE VSD + Dendritic Gating — Pancreatic Cancer
A: NIH Healthy (n=78) | B: MSD Adjacent (n=281) | C: MSD Tumor (n=281)
VSD sigmoid decomposition: 6 spectral channels → dendritic gating → 25 features
(A) VSD Feature Profiles
A: Healthy
B: Adjacent
C: Tumor
Response
(B) Effect Sizes
Cohen's d (A vs B)
(C) Feature Importance — A vs B
Importance
(D) ROC — VSD Feature Ablation
TPR
FPR
VSD z (6) AUC=0.926
z=struct (12) AUC=0.942
ALL 25 AUC=0.942
firing (6) AUC=0.776

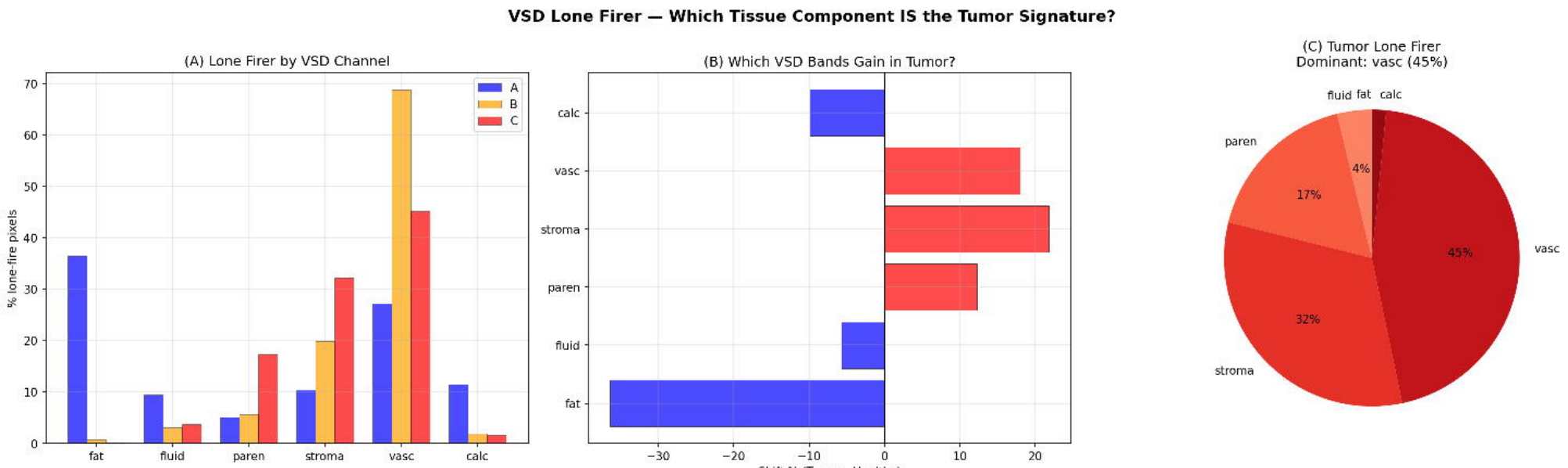
VSD Lone Firer — Which Tissue Component IS the Tumor Signature?
(A) Lone Firer by VSD Channel
% lone-fire pixels
A
B
C
fat
fluid
paren
stroma
vasc
calc
(B) Which VSD Bands Gain in Tumor?
Shift % (Tumor - Healthy)
(C) Tumor Lone Firer
Dominant: vasc (45%)
fluid
fat
calc
paren
4%
17%
45%
vasc
32%
stroma

VSD Early Detection — Progressive Detection Curves
Adding B patients from mildest to most severe: when does each feature become detectable?

(A) Progressive Detection Curves
Dots = first stable significance

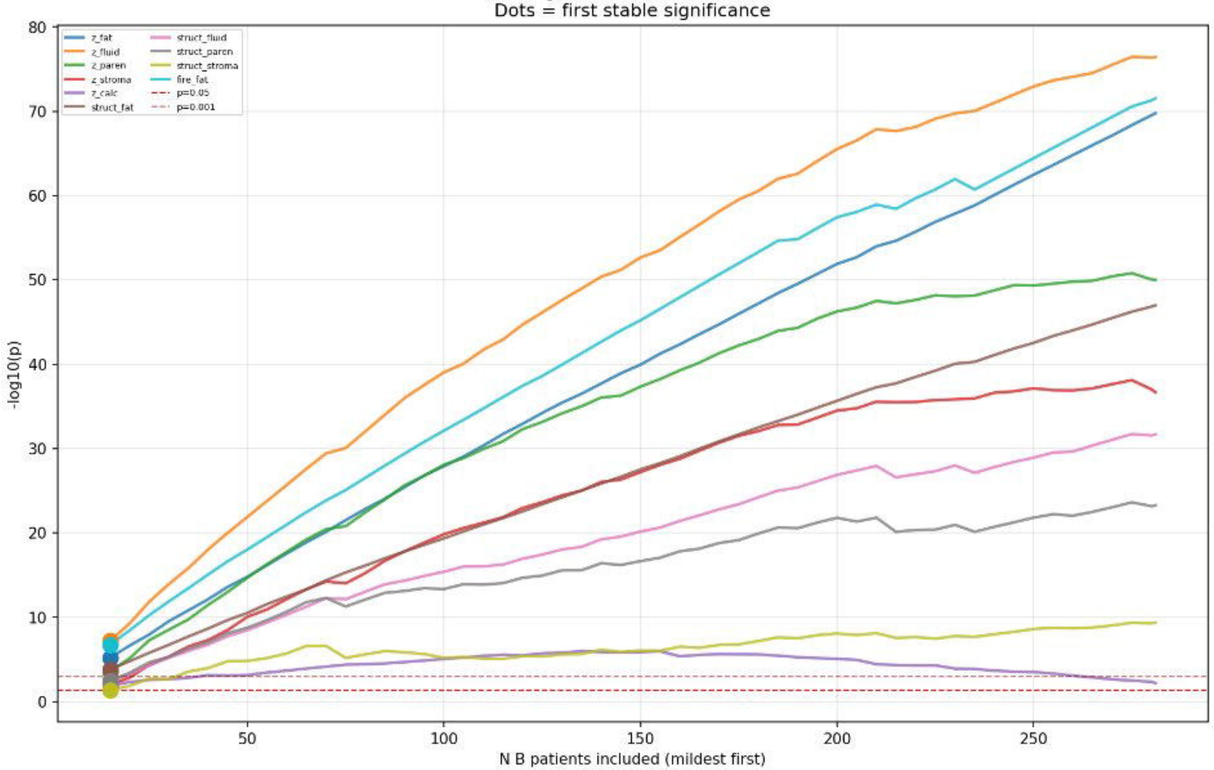

(B) Detection Order
Blue=z, Teal=struct, Coral=fire, Green=ratio

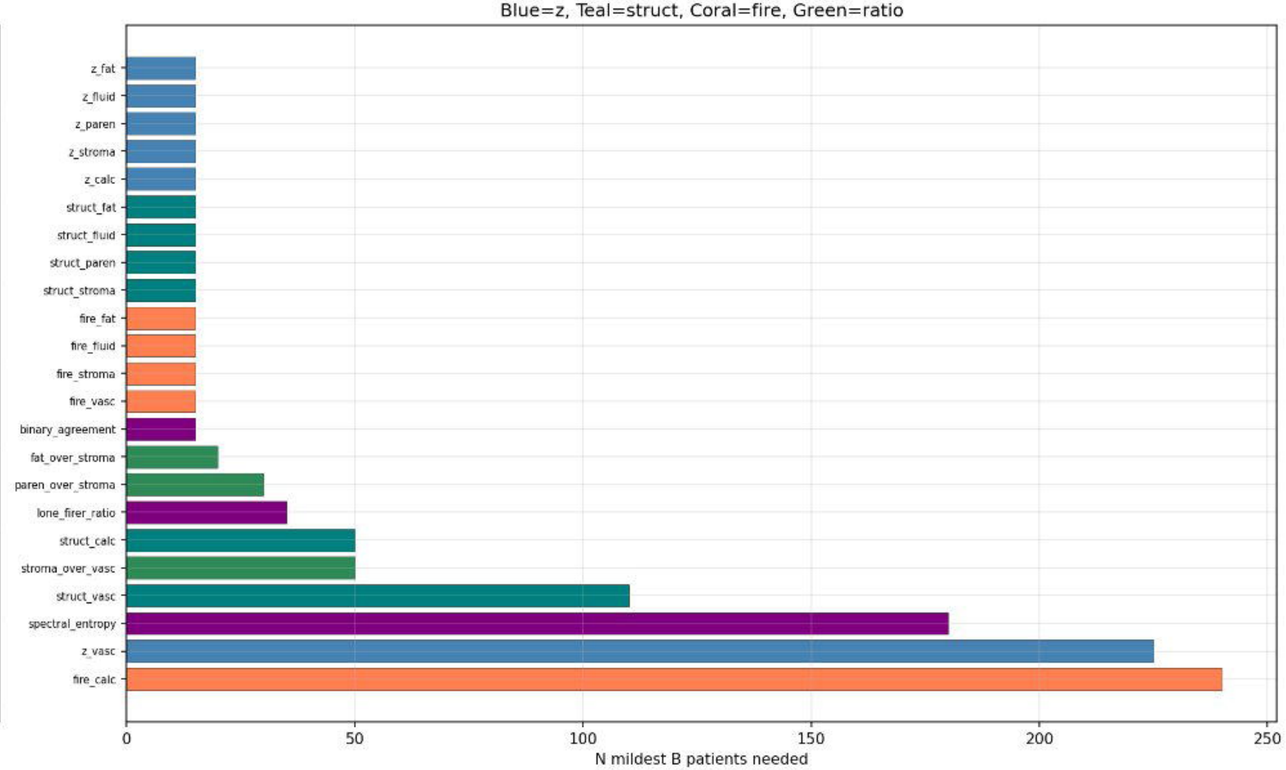

(C) VSD Z-Scores: 5-Stage Progression

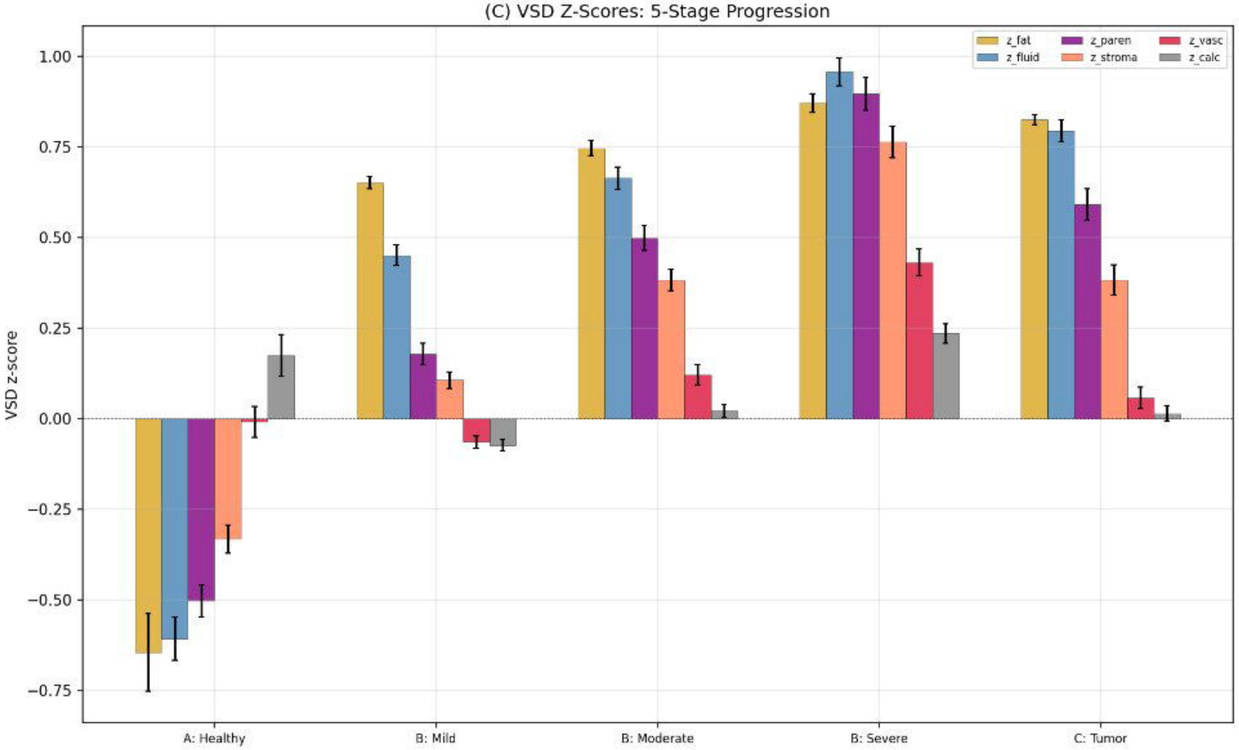

(D) Feature Activation Map (deciles)
Brighter = more significant

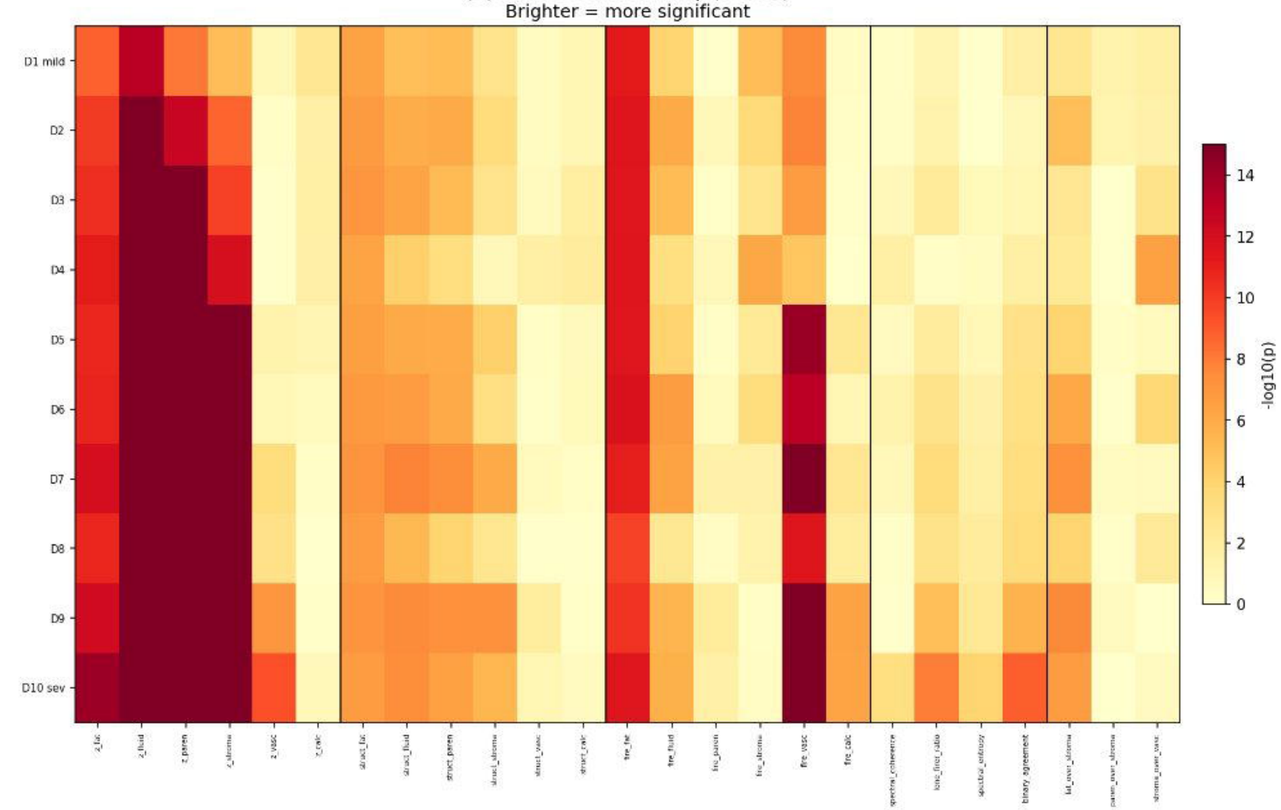

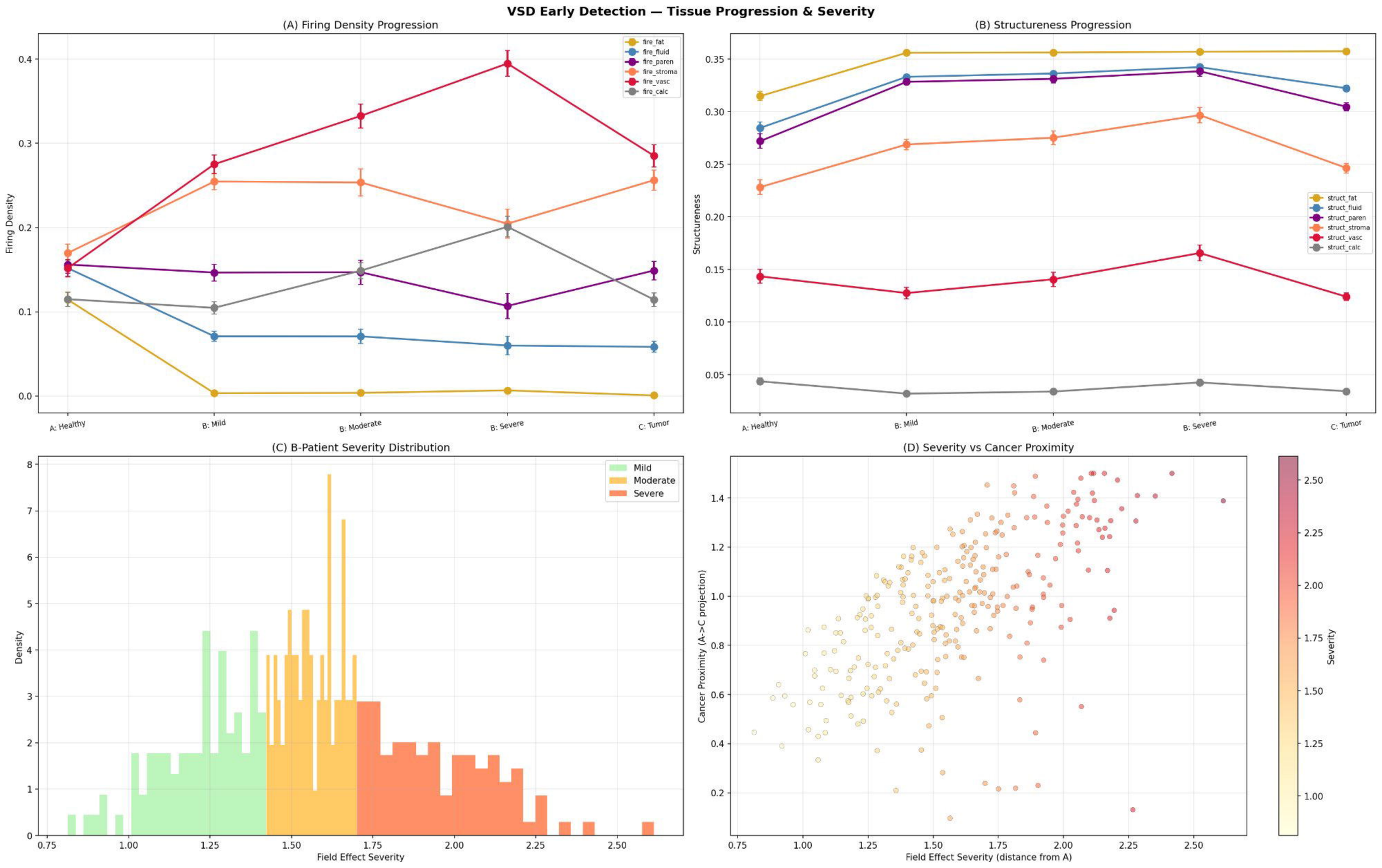
VSD Early Detection — Tissue Progression & Severity
(A) Firing Density Progression
Firing Density
fire_fat
fire_fluid
fire_paren
fire_stroma
fire_vasc
fire_calc
A: Healthy
B: Mild
B: Moderate
B: Severe
C: Tumor
(B) Structureness Progression
Structureness
struct_fat
struct_fluid
struct_paren
struct_stroma
struct_vasc
struct_calc
(C) B-Patient Severity Distribution
Density
Mild
Moderate
Severe
Field Effect Severity
(D) Severity vs Cancer Proximity
Cancer Proximity (A->C projection)
Field Effect Severity (distance from A)
Severity

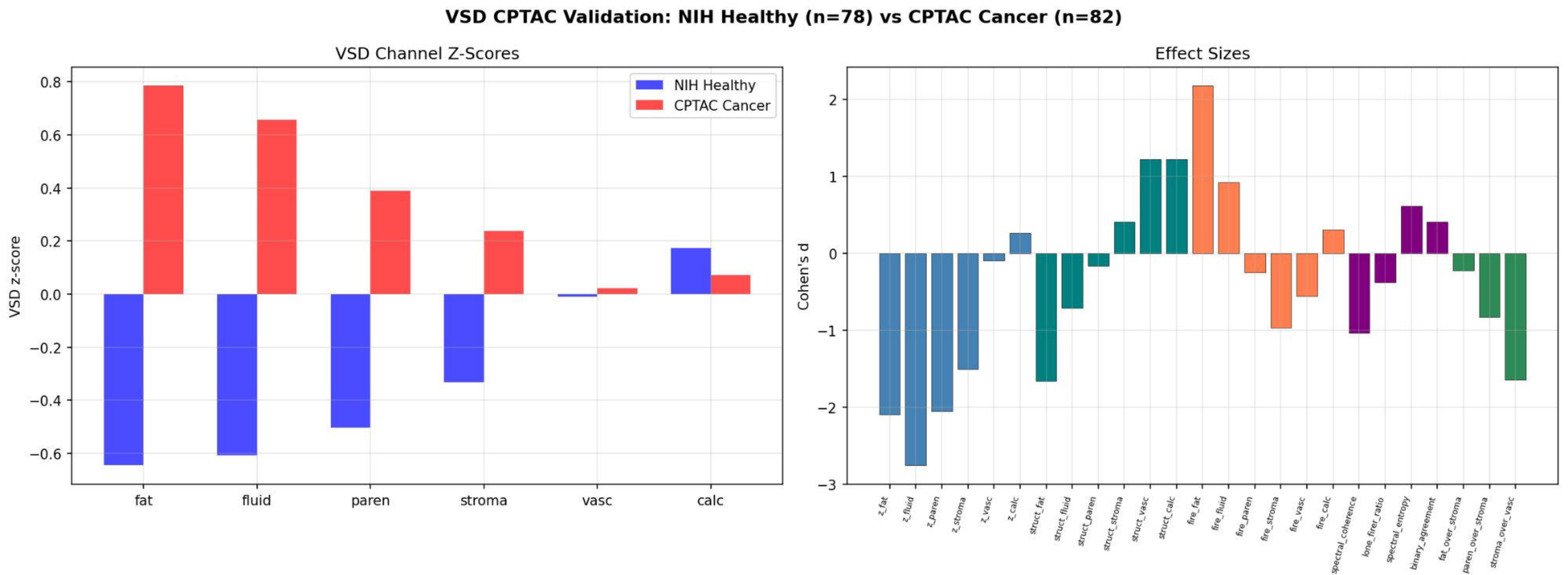
VSD CPTAC Validation: NIH Healthy (n=78) vs CPTAC Cancer (n=82)
VSD Channel Z-Scores
NIH Healthy
CPTAC Cancer
VSD z-score
0.8
0.6
0.4
0.2
0.0
−0.2
−0.4
−0.6
fat
fluid
paren
stroma
vasc
calc
Effect Sizes
Cohen's d
2
1
0
−1
−2
−3
z_fat
z_fluid
z_paren
z_stroma
z_vasc
z_calc
struct_fat
struct_fluid
struct_paren
struct_stroma
struct_vasc
struct_calc
fire_fat
fire_fluid
fire_paren
fire_stroma
fire_vasc
fire_calc
spectral_coherence
lone_firer_ratio
spectral_entropy
binary_agreement
fat_over_stroma
paren_over_stroma
stroma_over_vasc

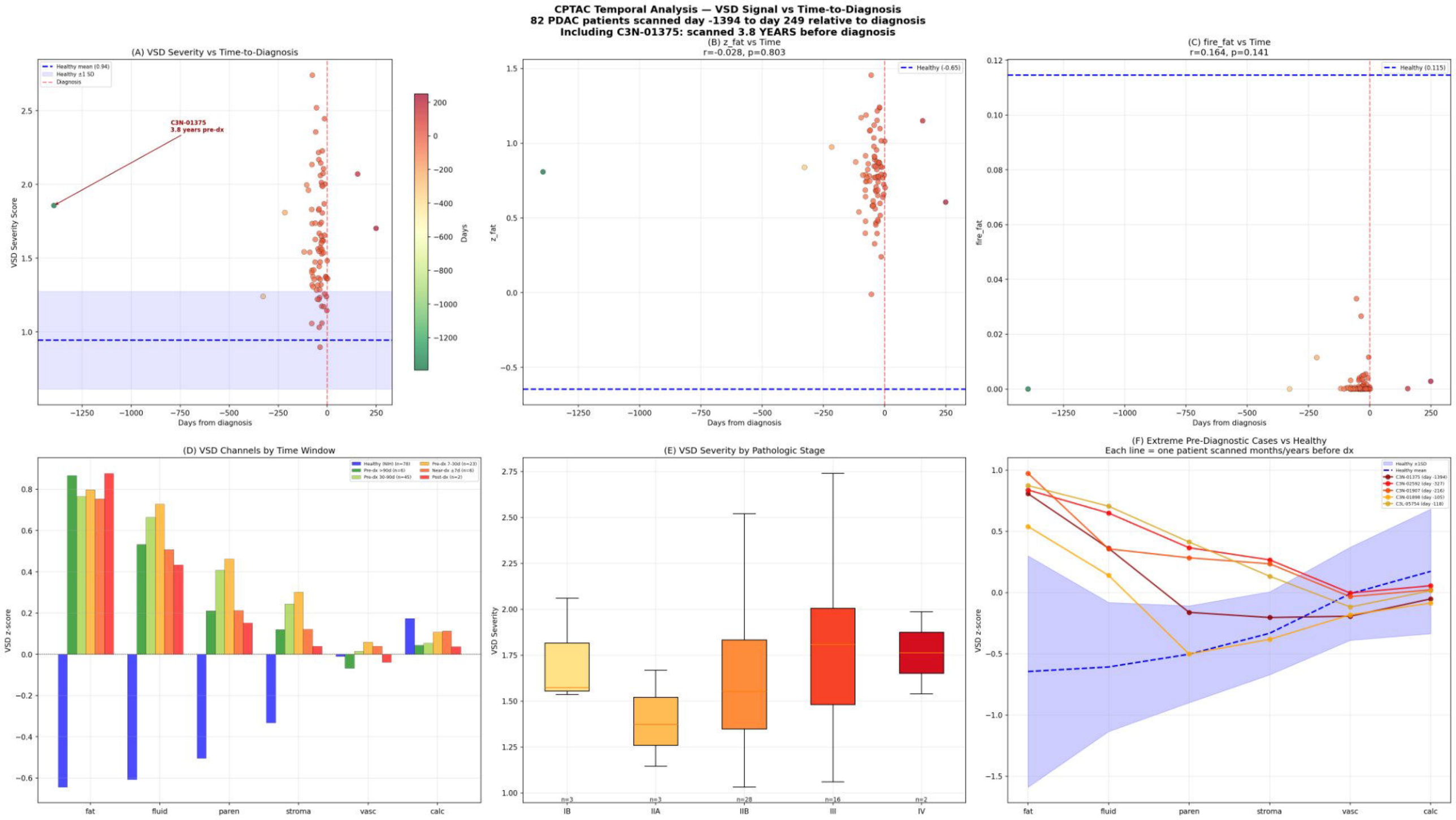
CPTAC Temporal Analysis — VSD Signal vs Time-to-Diagnosis
82 PDAC patients scanned day -1394 to day 249 relative to diagnosis
Including C3N-01375: scanned 3.8 YEARS before diagnosis
(A) VSD Severity vs Time-to-Diagnosis
Healthy mean (0.94)
Healthy ±1 SD
Diagnosis
C3N-01375
3.8 years pre-dx
VSD Severity Score
Days from diagnosis
Days
(B) z_fat vs Time
r=-0.028, p=0.803
Healthy (-0.65)
z_fat
Days from diagnosis
(C) fire_fat vs Time
r=0.164, p=0.141
Healthy (0.115)
fire_fat
Days from diagnosis
(D) VSD Channels by Time Window
Healthy (NIH) (n=78)
Pre-dx >90d (n=6)
Pre-dx 30-90d (n=45)
Pre-dx 7-30d (n=23)
Near-dx ±7d (n=6)
Post-dx (n=2)
VSD z-score
fat
fluid
paren
stroma
vasc
calc
(E) VSD Severity by Pathologic Stage
VSD Severity
n=3
n=3
n=28
n=16
n=2
IB
IIA
IIB
III
IV
(F) Extreme Pre-Diagnostic Cases vs Healthy
Each line = one patient scanned months/years before dx
Healthy ±1SD
Healthy mean
C3N-01375 (day -1394)
C3N-02592 (day -327)
C3N-01907 (day -216)
C3N-01898 (day -105)
C3L-05754 (day -118)
VSD z-score
fat
fluid
paren
stroma
vasc
calc